Version June 9, 2025
Preprint typeset using LaTeX style openjournal v. 09/06/15

TRINITY VII. PREDICTIONS FOR THE OBSERVABLE CORRELATION FUNCTIONS OF ACCRETING BLACK HOLES

Oddisey Knox[1], Haowen Zhang[1], and Peter Behroozi[1,2]
[1]Department of Astronomy and Steward Observatory, University of Arizona, Tucson, AZ 85721, USA and
[2]Division of Science, National Astronomical Observatory of Japan, 2-21-1 Osawa, Mitaka, Tokyo 181-8588, Japan
Version June 9, 2025

ABSTRACT

The quasar correlation function assesses the occurrence of quasar pairs as a function of separation, which is strongly influenced by quasar host halo masses. The empirical Trinity model recently inferred the redshift-dependent relationship between supermassive black hole (SMBH) mass, galaxy mass, and halo mass, using constraints other than correlation functions (e.g., quasar luminosity functions, active galactic nuclei occupation fractions, and SMBH mass–bulge mass relations). Hence, comparing the predicted quasar correlation functions from Trinity to real observations is an important test of Trinity's inferred SMBH—halo relation. In this work, we use a compilation of observed two-point projected and redshift-space correlation functions from $0 \leq z \leq 3.5$. We find that Trinity accurately predicts quasar correlation functions within observed error bars, although observations do not have much constraining power at lower redshifts due to smaller observable volumes and lower quasar number densities. This finding is consistent with Trinity having the correct placement of quasars within their host galaxies and dark matter halos, without requiring quasar clustering constraints during model fitting. Using Trinity, we also predict the clustering as a function of quasar bolometric luminosity, finding that existing survey uncertainties are too large to show measurable differences ($\lesssim 0.3$ dex change in bias for 10^{42} erg s^{-1} compared to 10^{46} erg s^{-1} SMBHs across redshifts). This fact arises because most SMBH growth (and hence quasar luminosity) occurs in halos in a similar mass range ($10^{12} - 10^{13} M_\odot$).
Subject headings: supermassive black holes – quasars – halos

1. INTRODUCTION

In the current paradigm of galaxy evolution, a galaxy forms in the center of each dark matter halo, and a supermassive black hole (SMBH) exists at the center of most galaxies (see, e.g., Silk & Mamon 2012; Somerville & Davé 2015; Naab & Ostriker 2017; Vogelsberger et al. 2020, for reviews). Yet, the physical processes by which galaxies and SMBHs grow and influence each others' growth remain uncertain. On the theoretical side, this has been due to the extreme simulation resolution required to model all relevant processes simultaneously, including gas infall on cosmological scales ($\gtrsim 1$ Mpc) and feedback from stars and the SMBH ($\lesssim 0.1$ pc). On the observational side, this has been due to the difficulty in making simultaneous observations of SMBHs in their most significant accretion phase (i.e., the quasar phase) along with their host galaxies, due to the quasar outshining the host galaxy. In the rare cases where this has been possible, the significant selection effects involved limit the information that can be inferred directly (even recently, e.g., Li et al. 2021).

At the same time, information about quasar host halos and galaxies is available from quasar environments. More massive halos and galaxies exhibit stronger spatial clustering due to the nature of structure formation in the Lambda Cold Dark Matter (ΛCDM) paradigm (e.g., Tinker et al. 2010; Wechsler & Tinker 2018). Hence, even when the host properties of quasars are not directly visible, their autocorrelation functions and cross-correlation functions with galaxies yield information on their host galaxies and dark matter halos. The most straightforward interpretation of the clustering yields both a characteristic host halo mass (typically $M_h \sim 10^{12} - 10^{13}\ M_\odot$, independent of quasar luminosity or redshift) and an inferred duty cycle, which is typically $\lesssim 0.1\%$, though this is highly dependent on sample selection (e.g., Croom et al. 2005; da Ângela et al. 2008; Ross et al. 2009; Shen et al. 2009; Eftekharzadeh et al. 2015; Chehade et al. 2016; Laurent et al. 2017).

Many models of SMBH evolution have hence used quasar correlation functions to constrain SMBH occupation in galaxies (e.g., Hopkins et al. 2008; Croton 2009; Shen 2009; Conroy & White 2013; Shankar et al. 2020a). The lack of luminosity dependence in quasar clustering most simply implies large scatter in the luminosity distribution of SMBHs, which is consistent with observations (e.g., Bongiorno et al. 2012; Aird et al. 2018). In addition, the lack of redshift dependence in the host halo mass most simply implies that most SMBH growth occurs in halos with $M_h \sim 10^{12} - 10^{13}\ M_\odot$, which is also the mass range hosting most galaxy growth (e.g., Moster et al. 2018; Behroozi et al. 2019).

We recently introduced an empirical model, Trinity, which uses an alternate approach to infer the halo–galaxy–SMBH relationship from observations (Zhang et al. 2023b). In Trinity, the halo–galaxy relationship is constrained primarily through observed galaxy number densities (see Wechsler & Tinker 2018, for a review), and halo growth histories in dark matter simulations then constrain galaxy growth histories. The galaxy–SMBH relationship is then primarily constrained by the $z = 0$ SMBH–galaxy relationship (specifically, the SMBH mass–galaxy bulge mass relationship; e.g., Häring & Rix 2004; Kormendy & Ho 2013; McConnell & Ma 2013) and the AGN luminosity distributions of galaxy progenitors at higher redshifts (as measured in Aird et al. 2018). In practice, this

gives similar information as applying the Sołtan argument to SMBHs in bins of $z = 0$ host galaxy stellar mass, summing AGN luminosity along galaxy growth histories to infer SMBH growth histories (see also Shankar et al. 2020b).

In this paper, we apply the best-fit halo–galaxy–SMBH relationship from Trinity to halos in a dark matter simulation and measure the resulting quasar autocorrelation functions. Of note, although Trinity combined many different data types to constrain SMBH and galaxy growth, it did not incorporate any quasar clustering data. Hence, the results here represent a pure prediction of the model. A match between Trinity's predictions and observations would suggest that the autocorrelation functions do not provide significant additional information about the SMBH–galaxy–halo relationship beyond that already in observed AGN luminosity distributions of galaxies. On the other hand, a mismatch would suggest that quasars and galaxies have a more complicated relationship, and that quasar correlation functions are key to interpreting it. We note that a similar test was performed in Aird & Coil (2021). In that paper, the authors compared to measured quasar biases; here, we compare to the full 2D projected and 3D redshift-space clustering as a function of distance scale. We also seek to understand, using predictions from Trinity, where the observed lack of luminosity dependence will begin to break down, and hence where quasar selection criteria will more strongly influence clustering (see also Powell et al. 2024).

In Section 2, we introduce the dark matter simulation used and relevant information about Trinity and the autocorrelation function calculation. In Section 3, we describe the observations to which we compare our predictions. In Section 4, we show the comparisons between Trinity's predictions and the observations. We discuss these results in Section 5 and conclude in Section 6. Throughout this paper, we assume a flat, ΛCDM cosmology with parameters $h = 0.67$, $\Omega_\Lambda = 0.693$, $\Omega_m = 0.307$, $n = 0.96$, and $\sigma_8 = 0.823$, consistent with the cosmology constraints in Planck Collaboration et al. (2016).

2. METHODS

2.1. *Dark Matter Simulations*

For this work, we use the *MultiDark Planck 2* simulation (*MDPL2*; Klypin et al. 2016; Rodríguez-Puebla et al. 2016) with a box size of 1000 comoving Mpc h^{-1}, 3840^3 particles, a mass resolution of $1.51 \times 10^9 M_\odot h^{-1}$, and a force resolution of 13 kpc h^{-1} at high redshifts and 5 kpc h^{-1} at low redshifts. The simulation was evolved from $z = 120$ until the present, and assumed a flat ΛCDM cosmology ($h = 0.67$, $\Omega_\Lambda = 0.693$, $\Omega_m = 0.307$, $n = 0.96$, and $\sigma_8 = 0.823$). Halos were found using the Rockstar halo finder (Behroozi et al. 2013a) and merger trees were constructed using the Consistent Trees code (Behroozi et al. 2013b). This simulation resolves all the halos expected to be hosting luminous quasars, while at the same time covering a large enough volume to minimize sample variance and have accurate large-scale clustering.

2.2. *The Trinity empirical model for supermassive black holes*

Trinity is a self-consistent, empirical model that infers the dark matter halo–galaxy–SMBH connection (Zhang et al. 2023b). Trinity begins with the distribution of dark matter halo masses as a function of redshift from an N-body simulation. From here, it parameterizes the scaling relations between halo, galaxy and SMBH masses, as well as the shape of the SMBH accretion rate distribution. Each point in this parameter space fully specifies a unique recipe to populate halos with galaxies and SMBHs as functions of the host halo's mass and redshift. For each trial point in parameter space, Trinity then predicts galaxy and SMBH properties in a mock universe and compares them with real observations. For galaxies, these observations include stellar mass functions, specific star formation rates, cosmic star formation rates, fractions of quiescent galaxies, and $z \geq 8$ UV luminosity functions. These data collectively cover a redshift range of $0 \leq z \leq 13$, including the latest $9 \leq z \leq 13$ galaxy UV luminosity functions from Harikane et al. (2023). For supermassive black holes, these observations include the $z = 0$ SMBH-bulge mass relation, active black hole mass functions, the quasar luminosity function, and active galactic nuclei (AGN) occupation fractions for all available redshifts in the range $0 \leq z \leq 6.5$. The difference between the predictions and observations determines the likelihood for each point in parameter space, and a Markov Chain Monte Carlo algorithm is used to generate new points in parameter space to explore. This approach results in the posterior distribution of SMBH–galaxy–halo relationships that match all observed data; in this study, we use the best-fitting relationship. As mentioned previously, no correlation function data constrained Trinity, so the results in this paper represent a pure model prediction.

2.3. *Computing quasar correlation functions*

We apply Trinity to the *MDPL2* simulation to generate the mock galaxy and SMBH catalogs used in this work. When constructing these catalogs, we determined the probabilities of galaxies hosting actively accreting BHs above a certain luminosity threshold based on the SMBH luminosity distribution predicted by Trinity:

$$f_{>L_{\rm thresh}}(M_h, z) = \int_{L_{\rm thresh}}^{\infty} P(L|M_h, z)\, dL\,, \tag{1}$$

where M_h is peak historical halo (or subhalo) mass and P is the luminosity distribution at a fixed halo mass and redshift from the best-fitting Trinity model. The luminosity distributions $P(L|M_h, z)$ from Trinity are consistent with the AGN observational data listed in Section 2.2, and are primarily constrained by the AGN occupation fraction in galaxies (giving $P(L|M_*, z)$) as well as galaxy number densities and correlation functions (giving $P(M_*|M_h, z)$). We then weight each halo and subhalo by $f_{>L_{\rm thresh}}(M_h, z)$ when calculating its contribution to the quasar two-point correlation function (2PCF). Intuitively, a longer fraction of time spent above the chosen luminosity threshold corresponds to a higher weight, and vice versa for a shorter fraction of the time (see also Aird & Coil 2021 for a similar approach). Because we compute quasar clustering based on the weights for all galaxies that may host a quasar (instead of those that stochastically light up as quasars at a single point in time), we can predict quasar clustering down to smaller scales (~0.2 Mpc) than measurable in most observational samples.

We compute the projected 2PCF by integrating the standard 3D correlation function:

$$w_p(R_p) = \int_{-\pi_{\rm max}}^{\pi_{\rm max}} \xi(R_p, \pi) d\pi. \tag{2}$$

Here, π is the line-of-sight distance including redshift-space distortions from peculiar motion, and R_p is the projected radius. The maximum line-of-sight distance, $\pi_{\rm max}$, was set to

TABLE 1
OBSERVATIONAL DATA SETS

Reference	2D/3D	Redshift Range	Selection	Survey Name	Area (deg^2)	Quasar Density (deg^{-2})
Croom et al. (2005)	3D	0.3 - 2.48	Optical	2QZ	721.6	31
da Ângela et al. (2008)	3D	0.3-2.9	Optical	2SLAQ	180	35
Ross et al. (2009)	2D+3D	0.3 - 2.1	Optical	SDSS DR5Q	4000	7.5
Eftekharzadeh et al. (2015)	2D+3D	2.2 - 3.4	Optical	SDSS III- BOSS	6950	10.6
Chehade et al. (2016)	3D	0.8 - 2.5	Optical	2QDESp, 2SLAQ, 2QZ, SDSS DR5	150-4000	8-67
Laurent et al. (2017)	3D	0.9 - 2.2	Optical	SDSS IV- eBOSS	1200	57

half the simulation box size, as there is relatively little difference in w_p for values of $\pi_{\rm max} > 60$ Mpc h^{-1}. The redshift-space 2PCF, $\xi(s)$, is also calculated in the standard way, by averaging $\xi(R_p, \pi)$ over the circle with $R_p^2 + \pi^2 = s^2$.

3. OBSERVATIONS

The observational data used in this paper are taken from the 2QZ (Smith et al. 2005), 2SLAQ (Richards et al. 2005), 2QDESp (Shanks et al. 2015), and SDSS surveys (York et al. 2000) (including DR5Q Schneider et al. 2007), SDSS III-BOSS (Eisenstein et al. 2011), and SDSS IV-eBOSS (Dawson et al. 2016). Observationally, it is difficult to find pairs of quasars on small scales due to the low number density of sources, so most observational constraints on autocorrelation functions are limited to scales greater than $\sim 1-2$ Mpc. See Table 1 for full details of the observational data sets, including detection method, redshift ranges, and sky areas. Typical luminosities of quasars in these observational samples are $L_{\rm bol} > 10^{46}$ ergs s^{-1} (Ross et al. 2009), with very little variation in quasar clustering with luminosity (e.g., Eftekharzadeh et al. 2015), and so we adopt $L_{\rm thresh} = 10^{46}$ ergs s^{-1} for comparison with TRINITY. When a given reference provides only luminosity-binned clustering without presenting a combined sample, we show the luminosity bin with least uncertainties in the main text, and show each luminosity bin individually in Appendix A.

4. RESULTS

The projected two-point correlation functions for the redshift range $0 < z < 3.5$ in bins of $\Delta z = 0.5$ are given in Figures 1 and 2. At $z < 1.5$, there is substantial uncertainty in the observed data points due to both smaller observable volumes and lower typical quasar luminosities, making the sample sizes much smaller. Constraints on the correlation function at and below this redshift prove more difficult than at higher redshifts, where quasars are more numerous. Therefore, all data points with uncertainties larger than 2 dex are shown with transparent hues in the figures. At higher redshifts, the data are more precise, as seen with da Ângela et al. (2008) at $\langle z \rangle = 1.5$ and Eftekharzadeh et al. (2015) at $z = 2.20 - 2.80$ and $z = 2.68$ from 1-10 Mpc. Overall, TRINITY's predictions agree well with observations within the uncertainties.

On large scales ($r_p \gg 10$ Mpc h^{-1}), there are known issues with calculating correlation functions that affect Eftekharzadeh et al. (2015), driven by difficulties in accounting for observational systematics at the required precision (including large-scale variations in number densities and survey depth). Per that author's suggestion (S. Eftekharzadeh, priv. comm.), we have limited the comparison to $r_p < 25$ Mpc/h. TRINITY predicts a downturn in the quasar autocorrelation function at similar scales ($r_p > 25$ Mpc/h) which is not an artifact of the model or box size; instead, this feature arises from the shape of the matter power spectrum and is universally found in N-body simulations regardless of size (e.g., Klypin et al. 2016).

The two-point redshift-space correlation functions are given in Figures 3 and 4. Many of the conclusions above also apply to redshift-space clustering. For example, at $z < 1.5$, there are few precise measurements of the quasar correlation function with which we can compare. At higher redshifts, $z \geq 2$, we see good agreement with both da Ângela et al. (2008) and Eftekharzadeh et al. (2015). In the case of Eftekharzadeh et al. (2015), BOSS reaches two magnitudes deeper than SDSS, resulting in 15 times as many quasars at $z \sim 2.5$. da Ângela et al. (2008), though covering a much smaller area, $\sim$180 deg^2, reaches much fainter magnitudes of $g = 21.85$ ($i \approx 21.45$), resulting in 8500 quasars. We see minor differences in downturns in the 3D correlation function of the observational data at low redshift-space separations, e.g., $z \lesssim 2.0$ at $\lesssim 5$ Mpc, and at slightly higher redshifts of $z = 2.0 - 3.0$ from $\sim 2-3$ Mpc. As this may be in part due to redshift uncertainties and systematic quasar–galaxy velocity offsets, we have tested adding a random scatter of 700 km s^{-1} in the redshift-space direction when computing $\xi(s)$ (the cyan curves in Figure 3 and Figure 4); this is similar to previous estimates (e.g., 690 km s^{-1} in Croom et al. 2005). We note that observational color cuts are not part of the selection criteria for TRINITY, which will inevitably result in some of the differences observed.

5. DISCUSSION

Overall, we see agreement between TRINITY and the observed correlation functions. This is consistent with a scenario in which TRINITY is already putting quasars in the appropriate host galaxies and host dark matter halos, without the need to use constraints from quasar clustering. We can interpret this intuitively by noting that quasar correlation functions do not change much with the luminosity threshold (see Fig. 5 and Appendix A). This arises because most of the quasars that are probed by optical surveys live in host halos and galaxies with very similar mass ranges ($M_h = 10^{12} - 10^{13} M_\odot$; see Paper III, Zhang et al. 2023a, which discusses the host halos and galaxies of quasars), and hence have similar clustering. The information about host halo occupancy is most likely already present in AGN occupation fractions (i.e., the fraction of galaxies of a given mass that host AGN of a given luminosity), given the finding in Aird & Coil 2021 that AGN occupation fractions applied to galaxy mock catalogs naturally reproduce quasar biases as a function of redshift. Indeed, AGN occupation fractions may be more constraining for physical models, as they also provide information on AGN in systems with much lower and much higher spatial clustering (and hence a wider range of host halo masses) than typical quasar samples.

Optical surveys use a wide variety of selection criteria that we cannot reproduce exactly, because there are substantial uncertainties in converting from the optical magnitude to the bolometric luminosity. Hence, different surveys could in prac-

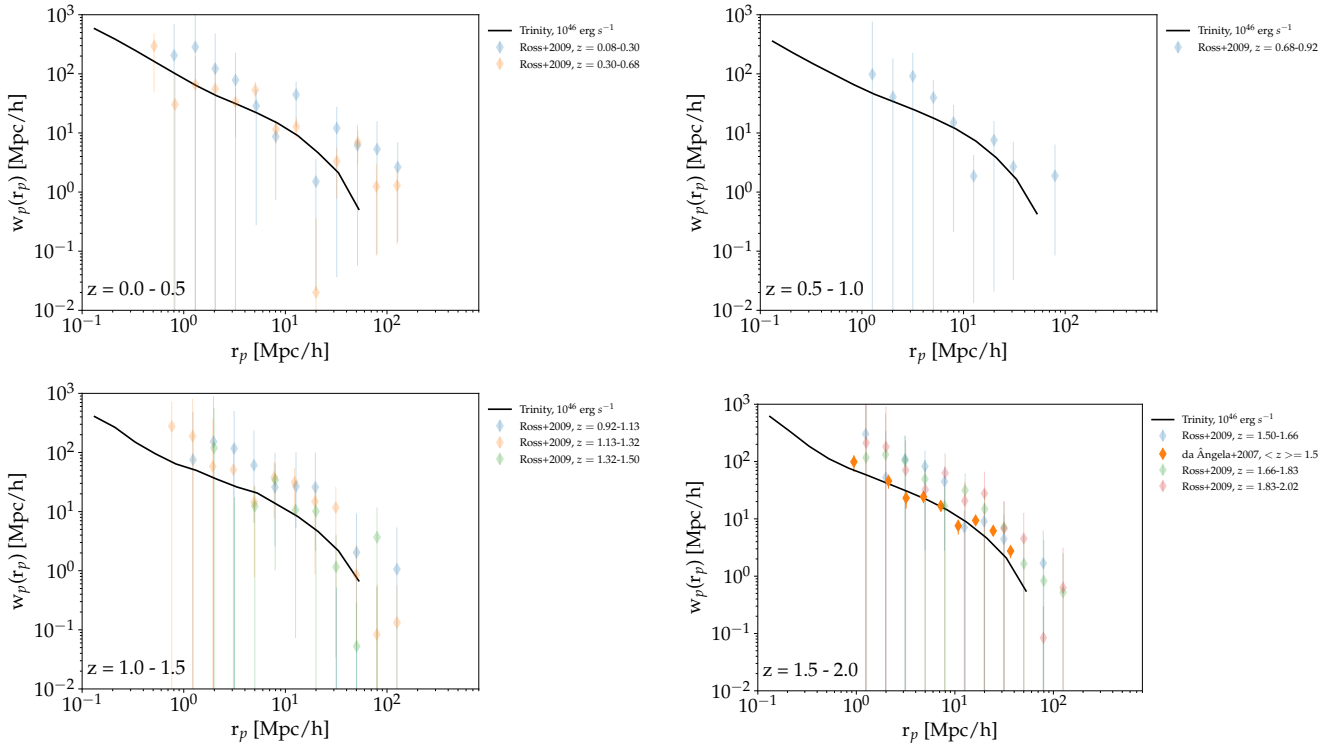

FIG. 1.— The two-point projected correlation function, w_p, for $z = 0 - 2$ in $\Delta z = 0.5$ bins. TRINITY predictions are shown as the black solid line, with observations shown as symbols. Observations with > 2 dex uncertainties are shown in transparent hues so that more precise measurements stand out visually.

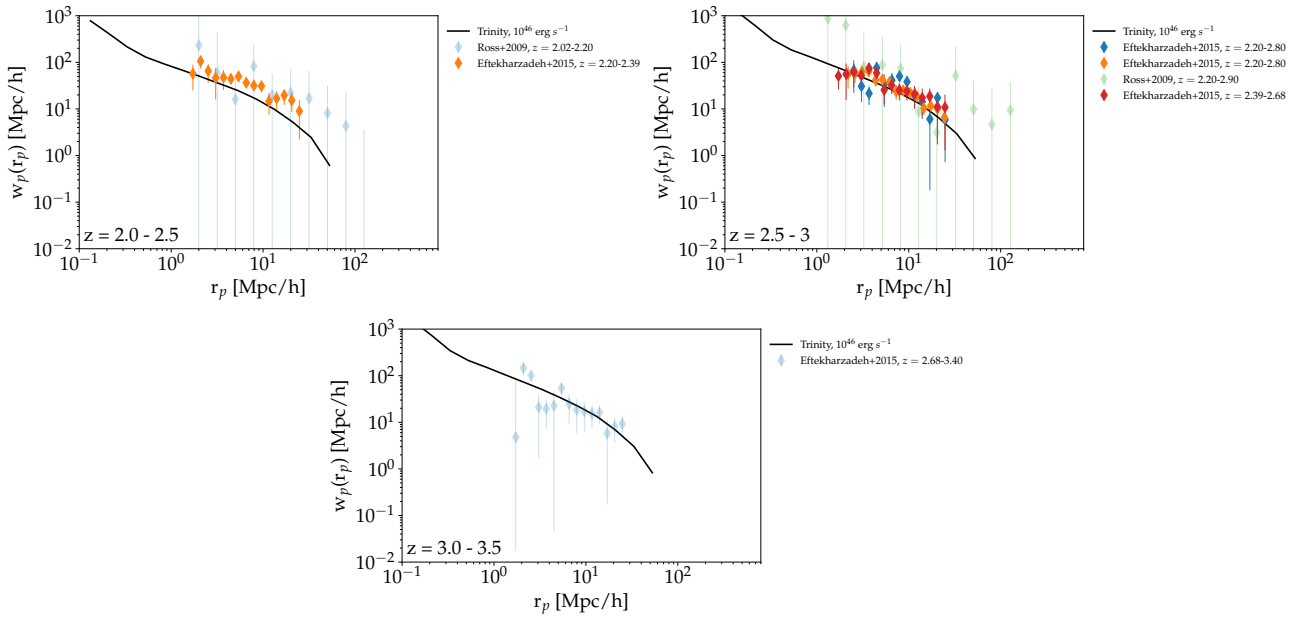

FIG. 2.— The two-point projected correlation function, w_p, for $z = 2 - 3.5$ in $\Delta z = 0.5$ bins. TRINITY predictions are shown as the black solid line, with observations shown as symbols. Observations with > 2 dex uncertainties are shown in lighter colors so that more precise measurements stand out visually.

tice be selecting quasar samples with very different bolometric luminosity distributions. Nonetheless, the observational samples with the tightest uncertainties agree both with each other and with the TRINITY model, which is reasonable given the weak correlation between total luminosity and clustering amplitude.

With new surveys probing fainter and fainter AGN (e.g., the BASS survey, Powell et al. 2018, the DESI $z \gtrsim 5$ Quasar Survey, Yang et al. 2023, as well as upcoming *Roman* and *Euclid* surveys), it is helpful to ask under what conditions luminosity-dependent quasar clustering will be observed. Fig. 5 (with additional redshifts in Appendix A) provides a simple answer: TRINITY predicts that there is typically < 0.3 dex variation in clustering down to very low luminosities (10^{42} erg/s). Most of the variation in quasar clustering occurs at high luminosities (between 10^{44-45} erg/s and 10^{46} erg/s or greater). But such systems are so rare that there are not enough of them to

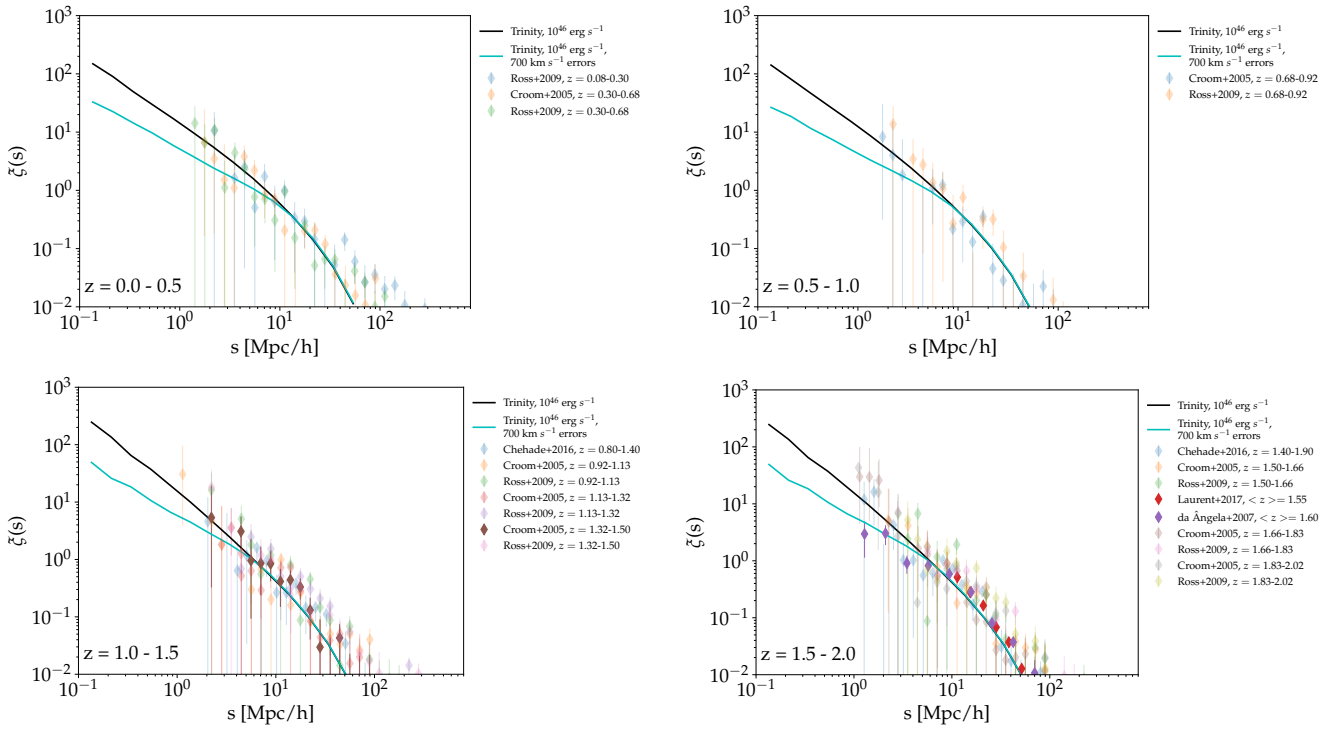

FIG. 3.— The 3D redshift-space correlation function, ξ_s, for $z = 0 - 2$ in $\Delta z = 0.5$ bins. TRINITY predictions are shown as the black solid line (no redshift-space errors) and the blue solid line (700 km s^{-1} redshift-space errors), with observations shown as symbols. Observations with > 2 dex uncertainties are shown in lighter colors so that more precise measurements stand out visually.

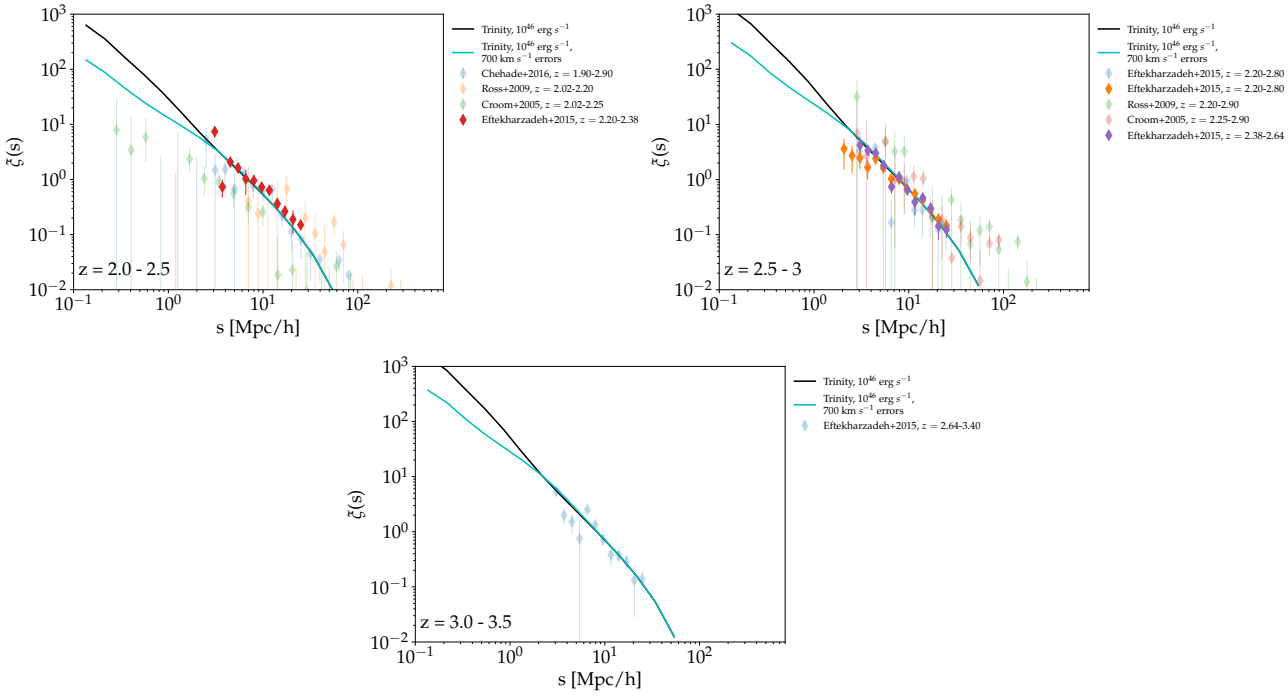

FIG. 4.— The 3D redshift-space correlation function, ξ_s, for $z = 2 - 3.5$ in $\Delta z = 0.5$ bins. TRINITY predictions are shown as the black solid line (no redshift-space errors) and the blue solid line (700 km s^{-1} redshift-space errors), with observations shown as symbols. Observations with > 2 dex uncertainties are shown in lighter colors so that more precise measurements stand out visually.

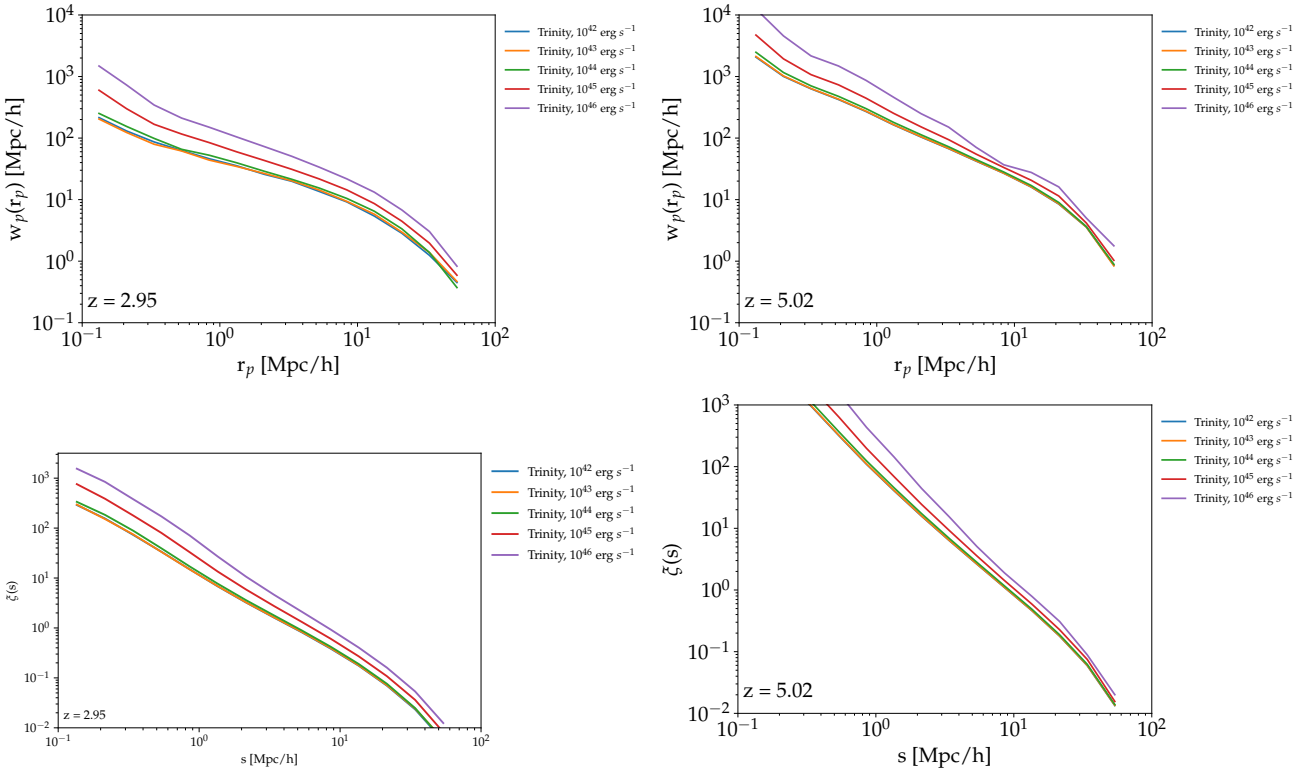

FIG. 5.— **Top**: Luminosity-dependent projected quasar clustering as predicted by TRINITY at $z \sim 3$ and $z \sim 5$. **Bottom**: Luminosity-dependent redshift-space quasar clustering as predicted by TRINITY at $z \sim 3$ and $z \sim 5$. In both cases, lower redshifts are shown in Appendix A; lower redshifts have even lower clustering differences between luminosity bins.

achieve tight constraints on quasar autocorrelation functions in the observable Universe. Another message from Fig. 5 is that the largest clustering differences are observed on small scales. Yet, given the low number densities of quasars, accessing small scales is difficult with autocorrelation functions. Both of these factors point to quasar-galaxy *cross-correlations* as the best route to measure luminosity-dependent clustering, so that the low number density of quasars does not pose an impediment to measuring clustering at high luminosities and small scales.

We can also speculate on why quasar clustering does not seem to depend on black hole mass (e.g., Krolewski & Eisenstein 2015). While in part this is due to uncertain virial estimates of black hole mass (see Krolewski & Eisenstein 2015), another factor is that selecting quasars already restricts the host halo mass range of the systems (see Paper III, Zhang et al. 2023a). Although we may expect lower-mass black holes to be hosted by lower-mass galaxies and halos, this is only true for the population as a whole. The tiny fraction of black holes that are accreting rapidly enough to shine as quasars are primarily living in $10^{12} - 10^{13} M_{\odot}$ halos—and hence, further splitting the quasar population in this already narrow range of halo masses (e.g., by black hole virial mass) does not result in large clustering differences (also known as the *restriction of range* effect in statistics).

6. CONCLUSIONS

In this paper, we compared predicted quasar autocorrelation functions from the TRINITY model with observed quasar autocorrelation functions for $0 < z < 3.5$. Key findings include:

- TRINITY agrees well with observed quasar autocorrelation functions, including their spatial dependence (Section 4). This is consistent with the interpretation that TRINITY is placing quasars in the appropriate galaxies and host halos (Section 5).
- As no quasar correlation functions were used to constrain TRINITY, this implies that galaxy and host halo occupation information was already present in another observational data set used for TRINITY–most likely AGN occupation fractions as a function of galaxy mass and redshift (Section 5).
- TRINITY predicts very shallow luminosity dependence for quasar clustering (Section 5), in agreement with observations (Appendix A). This is due to most quasars being hosted by halos in a very narrow mass range ($10^{12} - 10^{13} M_{\odot}$, almost regardless of selection).
- Future observations that target very bright quasars ($10^{46} - 10^{48}$ erg/s in bolometric luminosity) may have more success in finding luminosity dependent clustering by measuring small scale (< 5 Mpc) galaxy–quasar cross correlation functions, as quasar–quasar autocorrelation functions will be limited by low statistical power (Section 5).

ACKNOWLEDGEMENTS

OK would like to thank Bachem and Archie Knox for their unconditional patience through this process. OK would also like to thank Ann Zabludoff for her unwavering support on OK's journey to becoming a scientist. PB was funded by a Packard Fellowship, Grant #2019-69646.

REFERENCES

Aird J., Coil A. L., 2021, MNRAS, 502, 5962
Aird J., Coil A. L., Georgakakis A., 2018, MNRAS, 474, 1225
Behroozi P. S., Wechsler R. H., Wu H.-Y., 2013a, ApJ, 762, 109
Behroozi P. S., Wechsler R. H., Wu H.-Y., Busha M. T., Klypin A. A., Primack J. R., 2013b, ApJ, 763, 18
Behroozi P., Wechsler R. H., Hearin A. P., Conroy C., 2019, MNRAS, 488, 3143
Bongiorno A., et al., 2012, MNRAS, 427, 3103
Chehade B., et al., 2016, MNRAS, 459, 1179
Conroy C., White M., 2013, ApJ, 762, 70
Croom S. M., et al., 2005, MNRAS, 356, 415
Croton D. J., 2009, MNRAS, 394, 1109
Dawson K. S., et al., 2016, AJ, 151, 44
Eftekharzadeh S., et al., 2015, MNRAS, 453, 2779
Eisenstein D. J., et al., 2011, AJ, 142, 72
Harikane Y., Nakajima K., Ouchi M., Umeda H., Isobe Y., Ono Y., Xu Y., Zhang Y., 2023, arXiv e-prints, p. arXiv:2304.06658
Häring N., Rix H.-W., 2004, ApJ, 604, L89
Hopkins P. F., Hernquist L., Cox T. J., Kereš D., 2008, ApJS, 175, 356
Klypin A., Yepes G., Gottlöber S., Prada F., Heß S., 2016, MNRAS, 457, 4340
Kormendy J., Ho L. C., 2013, ARA&A, 51, 511
Krolewski A. G., Eisenstein D. J., 2015, ApJ, 803, 4
Laurent P., et al., 2017, J. Cosmology Astropart. Phys., 2017, 017
Li J., et al., 2021, ApJ, 922, 142
McConnell N. J., Ma C.-P., 2013, ApJ, 764, 184
Moster B. P., Naab T., White S. D. M., 2018, MNRAS, 477, 1822
Naab T., Ostriker J. P., 2017, ARA&A, 55, 59
Planck Collaboration et al., 2016, A&A, 594, A13
Powell M. C., et al., 2018, ApJ, 858, 110
Powell M. C., Krumpe M., Coil A., Miyaji T., 2024, arXiv e-prints, p. arXiv:2403.03978
Richards G. T., et al., 2005, MNRAS, 360, 839
Rodríguez-Puebla A., Behroozi P., Primack J., Klypin A., Lee C., Hellinger D., 2016, MNRAS, 462, 893
Ross N. P., et al., 2009, ApJ, 697, 1634
Schneider D. P., et al., 2007, AJ, 134, 102
Shankar F., et al., 2020a, Nature Astronomy, 4, 282
Shankar F., et al., 2020b, MNRAS, 493, 1500
Shanks T., et al., 2015, MNRAS, 451, 4238
Shen Y., 2009, ApJ, 704, 89
Shen Y., et al., 2009, ApJ, 697, 1656
Silk J., Mamon G. A., 2012, Research in Astronomy and Astrophysics, 12, 917
Smith R. J., Croom S. M., Boyle B. J., Shanks T., Miller L., Loaring N. S., 2005, MNRAS, 359, 57
Somerville R. S., Davé R., 2015, ARA&A, 53, 51
Tinker J. L., Robertson B. E., Kravtsov A. V., Klypin A., Warren M. S., Yepes G., Gottlöber S., 2010, ApJ, 724, 878
Vogelsberger M., Marinacci F., Torrey P., Puchwein E., 2020, Nature Reviews Physics, 2, 42
Wechsler R. H., Tinker J. L., 2018, ARA&A, 56, 435
Yang J., et al., 2023, ApJS, 269, 27
York D. G., et al., 2000, AJ, 120, 1579
Zhang H., Behroozi P., Volonteri M., Silk J., Fan X., Aird J., Yang J., Hopkins P. F., 2023a, arXiv e-prints, p. arXiv:2305.19315
Zhang H., Behroozi P., Volonteri M., Silk J., Fan X., Hopkins P. F., Yang J., Aird J., 2023b, MNRAS, 518, 2123
da Ângela J., et al., 2008, MNRAS, 383, 565

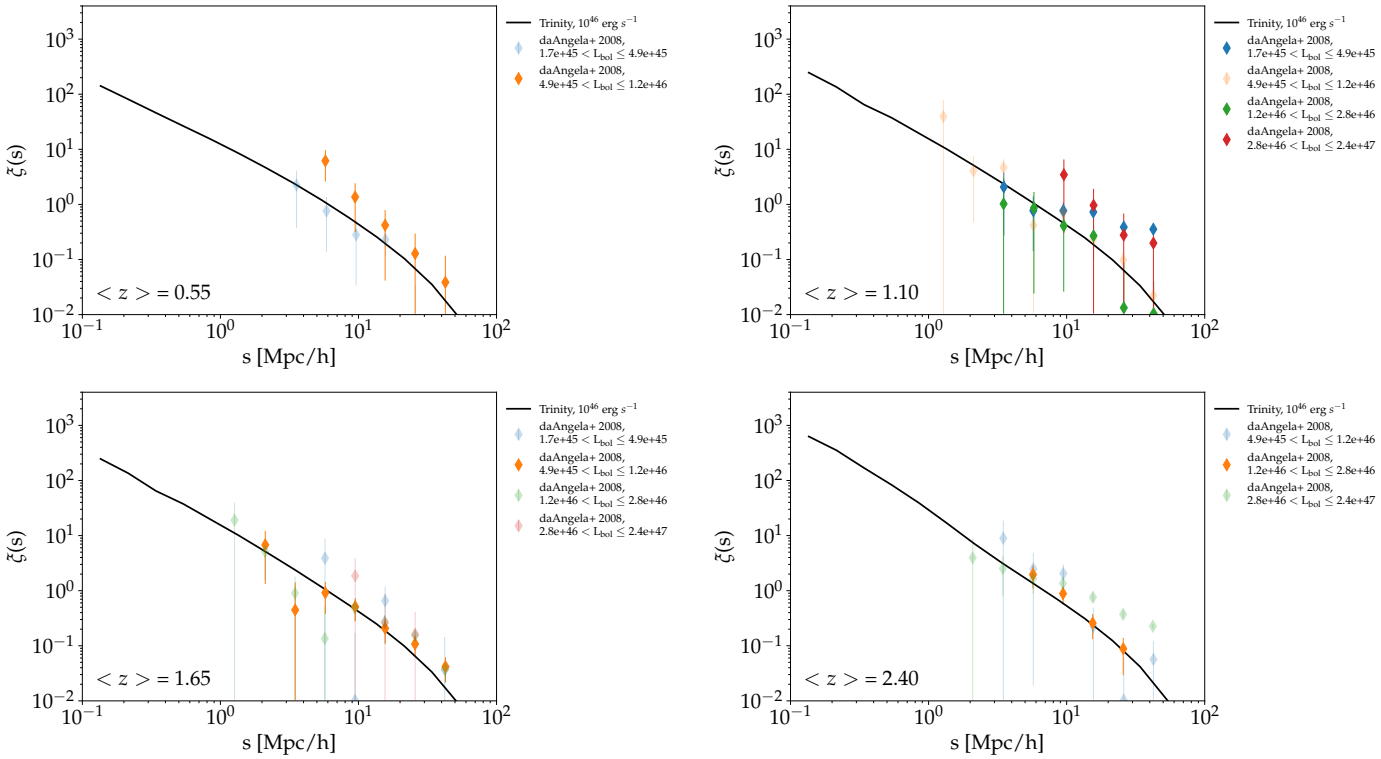

FIG. 6.— The 3D redshift-space correlation function, ξ_s plotted with da Ângela et al. (2008) luminosity-dependent observations.Observations with > 2 dex uncertainties are shown in transparent hues so that more precise measurements stand out visually.

APPENDIX

A. LUMINOSITY-BINNED QUASAR CLUSTERING

We show the da Ângela et al. (2008), Chehade et al. (2016), and Eftekharzadeh et al. (2015) luminosity clustering compared with TRINITY's predictions in Figs. 6–8. The observations show no evident luminosity dependence. The da Ângela et al. (2008) and Chehade et al. (2016) observations of the 3D redshift-space correlation function had average redshifts of $\langle z \rangle$ = 0.55, 1.10, 1.65, 2.40, and the Eftekharzadeh et al. (2015) data, for both the two-point projected and 3D redshift-space correlation function, were measured at $\langle z \rangle$ = 2.5. As expected from splitting observed samples, the observational error bars in the luminosity-split populations are larger in all cases compared to the whole-population constraints in Figs. 1–4, so it is not surprising that TRINITY's predictions continue to agree with the observations.

We show TRINITY's predictions for luminosity-dependent clustering at $z < 2.5$ in Figs. 9 and **??**. Compared to Fig. 5, lower redshifts show even less predicted luminosity dependence for quasar clustering, arising because the quasar population at lower redshifts is hosted by an even narrower typical range of halo masses than at higher redshifts (Zhang et al. 2023a). For this reason, we do not show separate TRINITY predictions for each luminosity bin in Figs. 6–8.

This paper was built using the Open Journal of Astrophysics LaTeX template. The OJA is a journal which provides fast and easy peer review for new papers in the astro-ph section of the arXiv, making the reviewing process simpler for authors and referees alike. Learn more at http://astro.theoj.org.

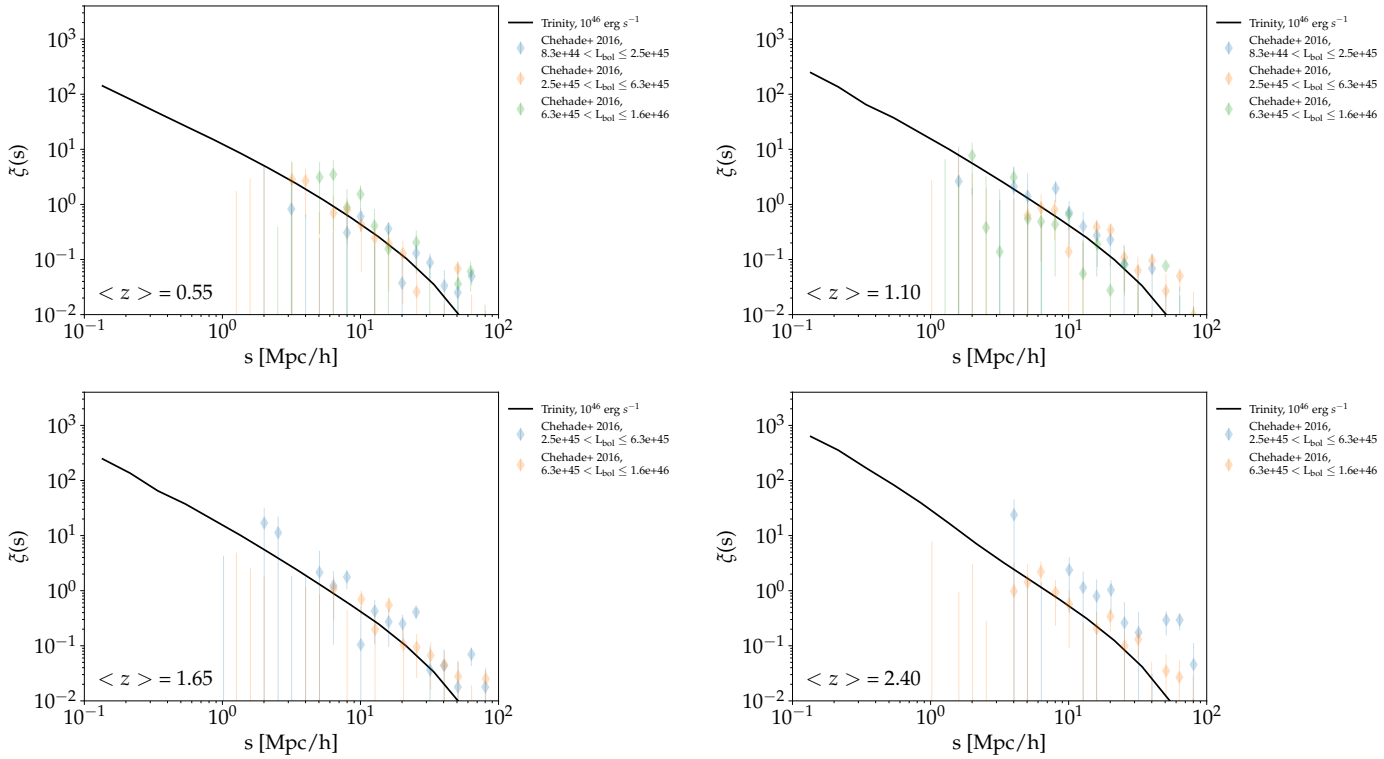

FIG. 7.— The 3D redshift-space correlation function, ξ_s plotted with Chehade et al. (2016) luminosity-dependent observations. Observations with > 2 dex uncertainties are shown in transparent hues so that more precise measurements stand out visually.

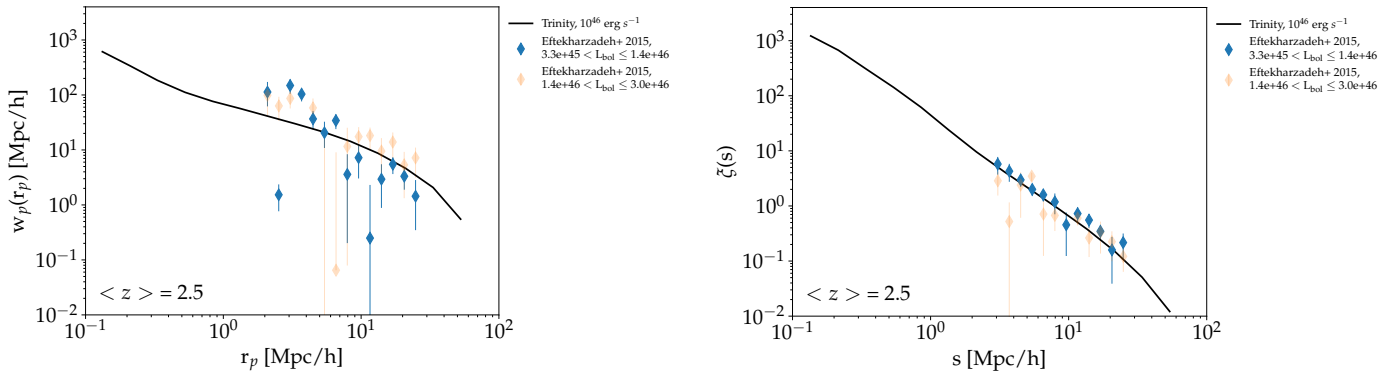

FIG. 8.— The two-point projected, w_p, and 3D redshift-space correlation functions, ξ_s plotted with Eftekharzadeh et al. (2015) luminosity-dependent observations at $< z = 2.5 >$. Observations with > 2 dex uncertainties are shown in transparent hues so that more precise measurements stand out visually.

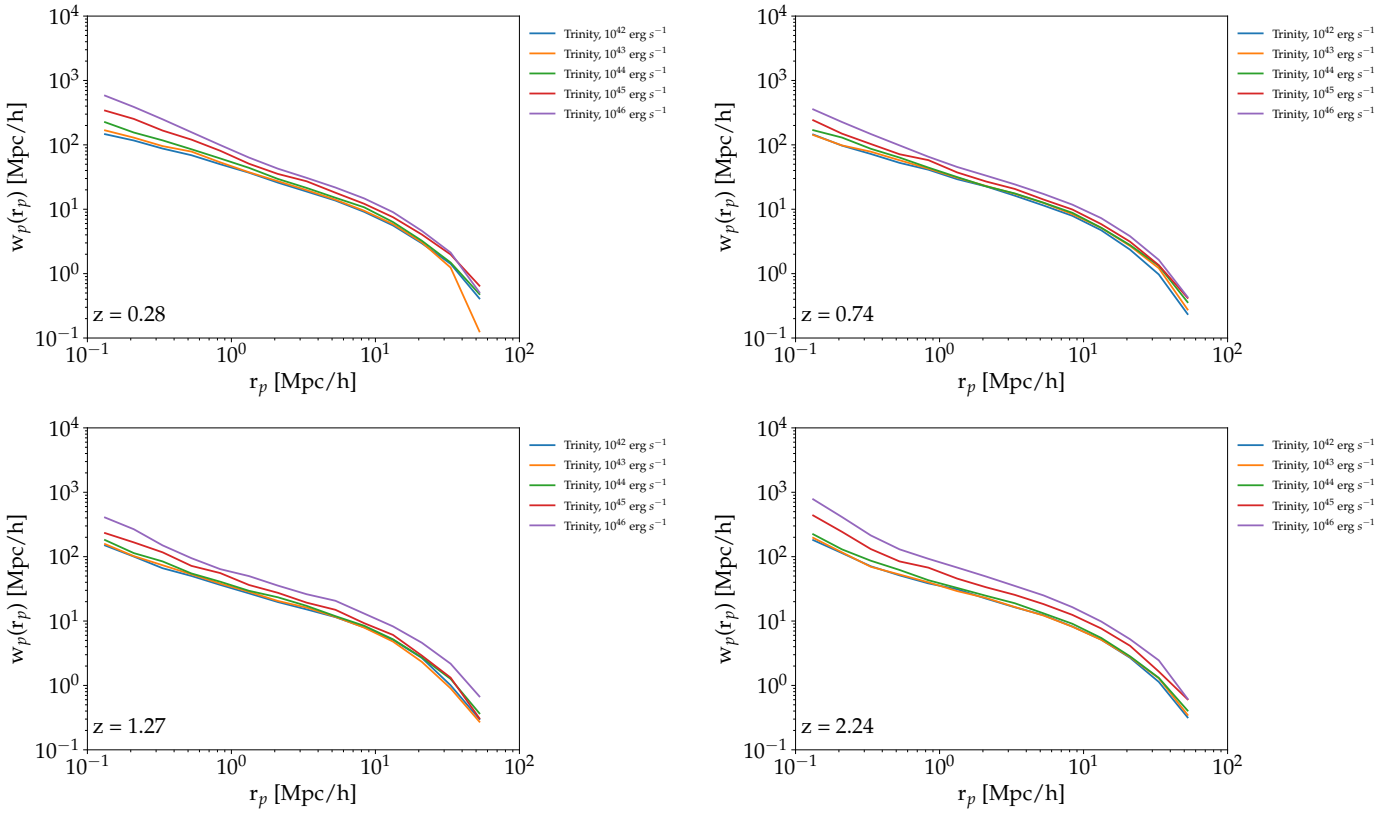

FIG. 9.— The two-point projected correlation function, w_p, for TRINITY from 10^{42} - 10^{46} erg s^{-1}. Each luminosity bin is represented by a different color.

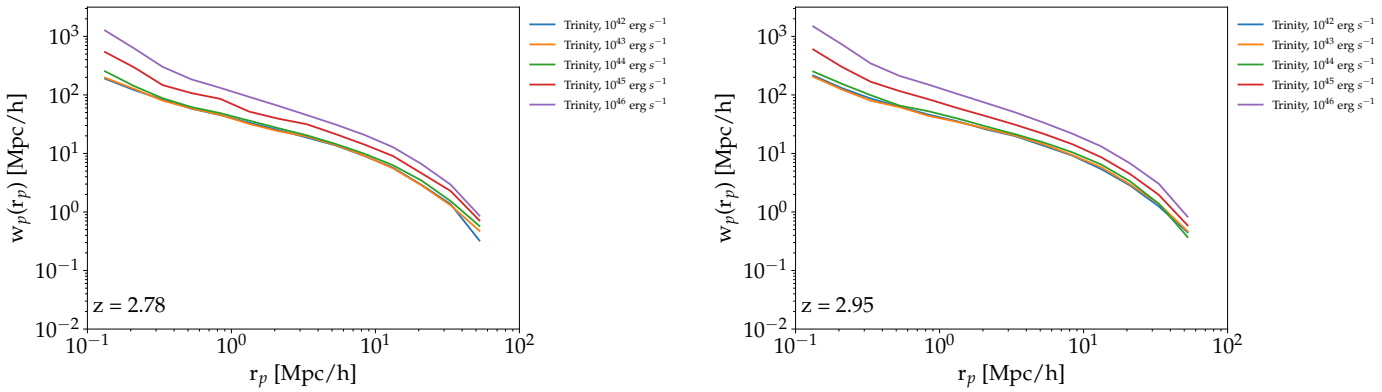

FIG. 10.— This is an example figure. Captions appear below each figure. Give enough detail for the reader to understand what they're looking at, but leave detailed discussion to the main body of the text.

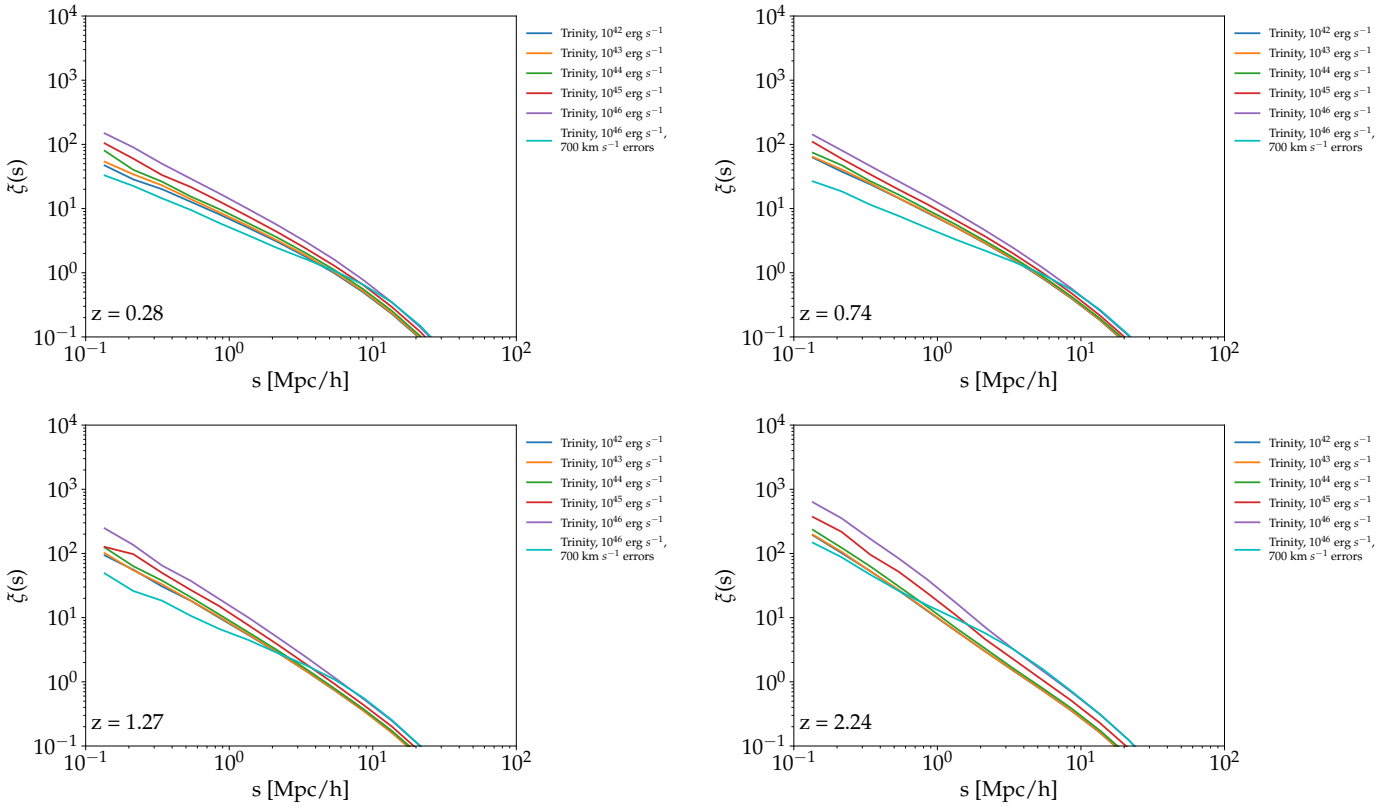

FIG. 11.— The 3D redshift-space correlation function, ξ_s, for TRINITY from 10^{42} - 10^{46} erg s^{-1}. Each luminosity bin is represented by a different color.